Astron. Astrophys. 316, 355–367 (1996)

ASTRONOMY
AND
ASTROPHYSICS

Constraints on high-speed solar wind structure near its coronal base: a Ulysses perspective

W.C. Feldman[1], **B.L. Barraclough**[1], **J.L. Phillips**[1], **and Y.-M. Wang**[2]

[1] Los Alamos National Laboratory, MS D466, Los Alamos, NM 87545, USA
[2] E.O. Hulburt Center for Space Research, Naval Research Laboratory, USA

Received 10 February 1996 / Accepted 2 May 1996

Abstract. Ulysses plasma data at high heliographic latitudes were studied to develop constraints on the structure of the corona at the base of the high-speed solar wind. Salient features of the flow poleward of $\pm 60^\circ$ revealed: 1) low variances of all bulk flow parameters, 2) parameter values that agree with those measured during high-speed conditions in the ecliptic plane when all are scaled to 1 AU, 3) the continuous presence of two interpenetrating proton streams that are not resolved in velocity space, 4) a single alpha-particle beam that travels at a speed that is close to the local Alfvén speed faster than the primary proton beam, 5) a proton temperature that is a factor of 2.4 times that of the electrons, and 6) a constant helium abundance that averages 4.4% , about half that inferred from helioseismic data in the solar convection zone. These data are combined with a host of other remote-sensing solar data and solar wind data to develop support for a model of a well-mixed solar atmosphere that is driven by reconnection-generated plasma-jet transients. In this model, acceleration of the solar wind to its terminal speed is complete within a heliocentric distance of about $5\,R_s$.

Key words: solar wind – Sun: corona

1. Introduction

The structure of the solar corona within holes at the base of the high-speed solar wind is basically not known. This lack of knowledge stems from essential ambiguities in interpretations of all remote-sensing observations used exclusively in the past to infer conditions within the chromosphere-corona transition region and the low corona. They include EUV imaging and spectroscopy observations of the Sun from 1 AU, observations of interplanetary scintillations (IPS) from Earth, and plasma and magnetic field observations of the solar wind between 0.3 and 1 AU in the ecliptic plane. (Observations of the solar wind beyond 1 AU reveal more about interplanetary processes than they do about the structure of the corona.) Nevertheless, the currently accepted paradigm for conditions at the base of the high-speed solar wind postulates a relatively time-stationary, uniform, low density ($\sim 10^8\,cm^{-3}$), low electron temperature ($\sim 10^6$ K), high proton temperature (10^7 K), and high speed ($\sim 800\,km\,s^{-1}$) flow (McKenzie et al. 1995). Introduction of Alfvén waves having a $20\,km\,s^{-1}$ velocity amplitude at the coronal base reduces the requirement for such a large peak coronal proton temperature to about 2×10^6 K (Habbal et al. 1995). Also postulated is a heavy-ion flow state that is characterized by a temperature proportional to ion mass and a speed faster than that of the protons by as much as the local Alfvén speed. The energy flux needed to support this state is assumed to come from the damping of Alfvén waves generated by small- scale activity within the chromospheric network just above the photosphere (Axford & McKenzie 1992).

However, the foregoing paradigm is not complete, as shown by an increasing number of solar and solar wind observations, namely; 1) Explosive events seen most prominantly at $T \sim 10^5$ K drive upward-going plasma jets at a rate of more than 7.6 per day on every open magnetic field line that connects the photosphere to interplanetary space (Dere 1994). These jets are time-dependent injections of high-speed plasma having a continuum of speeds up to some maximum. They have a fine structure characterized by a volumetric fill factor of 10^{-4} and should produce velocity-resolved peaks at their leading edges in much the same way as happens in Type III radio bursts. 2) Measurements of the hydrogen Lyα line shape at $1.8\,R_s$ in a polar hole are consistent with a two-component corona comprising a thermal component having $T = 1.6 \times 10^6$ K superimposed on a $\sim 60\%$ admixture of hydrogen atoms having non- thermal velocities perpendicular to B of about $300\,km\,s^{-1}$ (Kohl et al. 1995). 3) IPS measurements at a closest-approach distance of less than $5\,R_s$ through a polar coronal hole reveal field-aligned density structures having a 10:1 radially-aligned axial ratio, and apparent field-aligned speeds that range between about 400 and $1280\,km\,s^{-1}$ (Coles et al. 1991; Klinglesmith et al. 1995; Grall et al. 1996). And finally, 4) observations of two relatively streaming proton components, coupled with a single, faster-moving

Send offprint requests to: W.C. Feldman

alpha-particle beam, are consistent with existence of an ensemble of fast plasma jets in the low corona that comprise between 20% and 25% of the integrated mass flux density of the high-speed solar wind (Feldman et al. 1976a, 1993).

Until recently, inference of coronal conditions at the base of the high-speed solar wind came from measurements of the solar wind at relatively large heliocentric distances near the equatorward margins of large coronal holes that were topologically connected to either of the solar magnetic poles (Feldman et al. 1976b; Bame et al. 1977; Schwenn, 1991). In consequence, it was not possible to conclusively eliminate effects on the observed flow state introduced by proximity to the streamer belt that encircles the Sun near its magnetic equator. This limitation has now been removed with the availability of Ulysses observations that cover heliographic latitudes between $\pm 80.2^\circ$ during a period that is close to solar minimum coronal conditions. Indeed, Ulysses spent more than 650 days (between launch in October, 1990 and November, 1995) within the high-latitude wind, which came from two large coronal holes that capped the Sun at latitudes poleward of $\pm 40^\circ$. In Sect. 2 of this paper we present a selection of data from the ion and electron plasma spectrometers of the Ulysses solar wind experiment (Bame et al. 1992) that bears on coronal conditions at the base of the high-latitude solar wind. These data are then interpreted in Sect. 3 to develop constraints on conditions at the base of the solar wind. They are also compared with other conditions inferred from observations of the chromosphere-corona transition region using EUV imaging and spectroscopy experiments, and of the high corona using IPS data. Our study is summarized in Sect. 4.

2. Observations

2.1. Overview

An overview of solar wind conditions sampled by Ulysses between launch and 4 November, 1995 is presented in Fig. 1. The various flow states that were encountered are best distinguished by the bulk flow speed shown at the top of each of the two panels stacked vertically in the figure. The relative abundance of helium, $[He] = N_{He}/N_H$, is plotted at the bottom of both panels for later reference. Launch occurred during solar maximum, resulting in encounter of generally low speed flow conditions punctuated by occasional coronal mass ejections (CMEs) throughout the ecliptic portion of the mission (from November, 1990 to about June, 1992, Phillips et al. 1995a). Soon afterwards, Ulysses began a period of partial penetration into the high-speed wind that evolved from the large coronal hole that covered the Sun's south polar magnetic cap, which at that time was displaced from the Sun's rotation axis by about 30° (Bame et al. 1993). Ulysses remained within a relatively structure-free, high- speed flow regime (median speed increased slowly with latitude from about $740\,km\,s^{-1}$ at the margins of the polar cap to about $780\,km\,s^{-1}$ at $\pm$ 80.2°) poleward of about $\pm 40^\circ$ until the end of our data set, arbitrarily cut off for the purposes of this study in November, 1995. This regime was marked by: 1) a relatively low and constant density when scaled to 1 AU (Phillips et al. 1995b), 2) a relatively high and constant helium abundance (Barraclough et al. 1996), and 3) a large-amplitude field of Alfvén waves that increased gradually from a relatively low intensity at the margins of the polar cap to a high and relatively constant intensity poleward of about $\pm 60^\circ$ (Balogh et al. 1995). The period of generally low and variable speed wind measured during early March, 1995, corresponded to passage through the extension of the coronal streamer belt, which at this time covered an approximately $\pm 21^\circ$ latitude range centered about the heliographic equator (Gosling et al. 1995).

2.2. Coronal magnetic expansion factor

The main task of this study is to make a correspondence between Ulysses observations of the solar wind far from the Sun, to conditions within the polar coronal holes at the base of the high-speed solar wind. We will therefore concentrate on plasma quantities that are constants of the motion along stream flow lines. These include: 1) the mass flux, 2) the total energy flux, and 3) the helium abundance. However, in order to translate the solar wind mass and energy fluxes to conditions at the base of the corona, we require knowledge of the area-expansion factor from the coronal base to the altitude at which stream lines become radial. This factor was estimated by Gosling et al. (1995) to average 4.8 during the Ulysses rapid latitude scan. It was derived from the facts that: 1) the holes covering both polar caps were observed to occupy only about 13% of the low corona, yet 2) the high-speed solar wind was measured over a latitude range that corresponded to 63% of the sphere at 1 AU.

It is possible to refine this estimate further by combining the constancy of the radial component of the magnetic field measured by Ulysses (when scaled by R^{-2} to 1 AU, Balogh et al. 1995), with a model of the current-free expansion of the photospheric magnetic field. Previous experience with this model (see, e.g., Wang & Sheeley 1990) leads us to expect the highest accuracy by confining our determination of mass and energy flux to a rather narrow latitude range centered about the heliomagnetic poles. This choice also avoids the possible contamination of measured fluxes by the poleward edges of density compressions driven by corotating interaction regions, which were observed to extend to as high as -60° during the southern latitude portion of the Ulysses trajectory (Phillips et al. 1995b). We will therefore confine our estimation of the mass and energy flux at the base of the high- speed solar wind to data that was measured poleward of $\pm 60^\circ$ heliographic latitude.

Averages of the net area expansion factor between the coronal footpoints and Ulysses were calculated using the combined potential-field source-surface and equatorial current-sheet model of Wang and Sheeley (1995). The photospheric magnetic field, derived by deprojecting the line-of-sight field measured by the Wilcox Solar Observatory, provided the lower boundary conditions for this model. A radius of $2.5\,R_s$ was used for the source surface. Expansion factors were calculated for every 5° of Carrington longitude at the heliographic latitude of Ulysses. A histogram of these factors for times when Ulysses was poleward of $\pm 60^\circ$ is given in Fig. 2. The distribution is seen to be

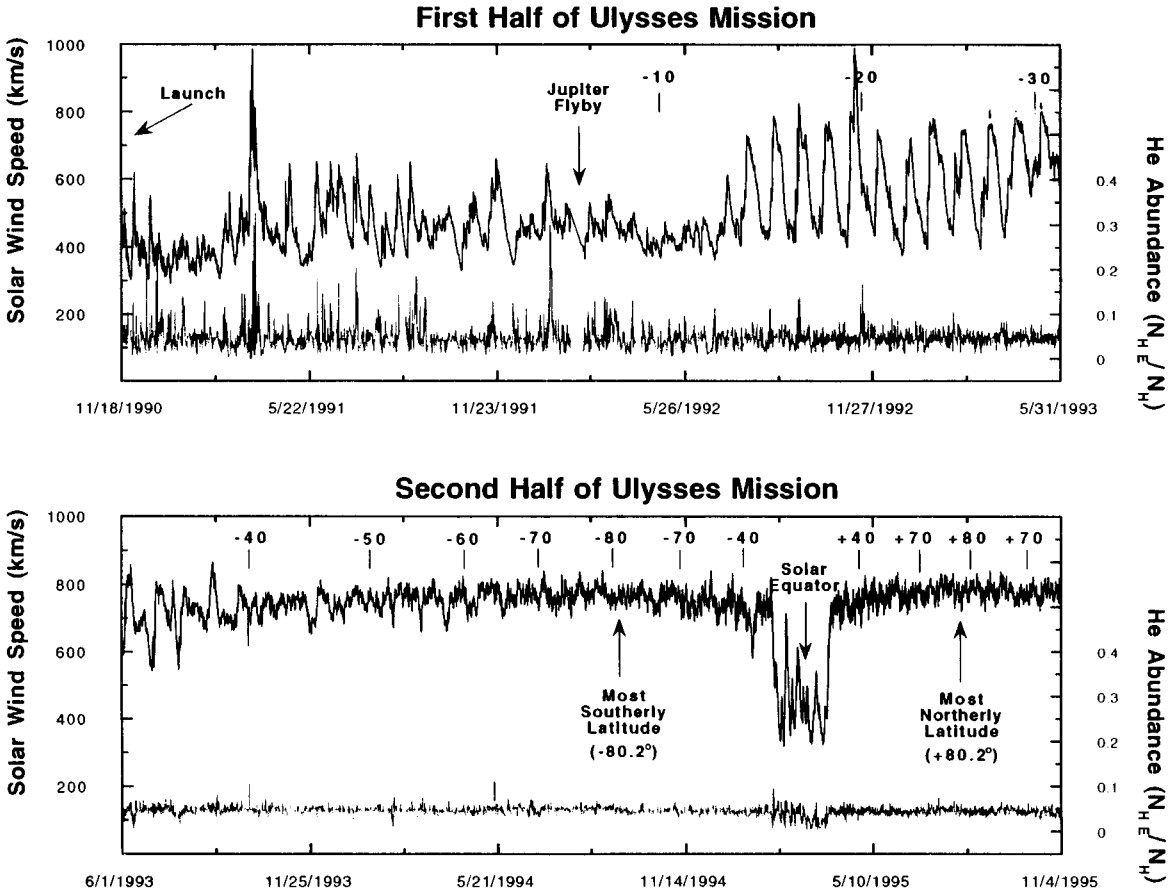

Fig. 1. Hourly averages of the solar wind bulk speed (upper trace) and helium abundance (lower trace) measured by the plasma experiment aboard Ulysses between 18 November, 1990, and 4 November, 1995. Heliographic latitude is given at the top of each panel

relatively narrow with a mean of 11.0 ± 1.3, and a median of 10.9. Both of these estimates are more than twice the average expansion factor estimated by Gosling et al. (1995) for the entire polar caps. The cause of this discrepancy is that the measured large magnitude of the Sun's polar magnetic field enforces a large net over-expansion of the field lines above the solar magnetic poles, and a corresponding relative compression of field lines at the margins of the polar coronal holes where they interface with the extension of the streamer belt. We believe this over- expansion to be real and will therefore use a factor of 11 to make the correspondence between the 1 AU-scaled Ulysses mass and energy fluxes presented next, and their values at the base of the high-latitude solar wind.

2.3. Bulk flow parameters of the high-latitude solar wind

Previous studies of Ulysses data to search for monotonic variations of bulk flow parameters with heliographic latitude yielded generally negative results (see, e.g., Feldman et al. 1996, and references therein). The only significant variation that has been documented is a relatively small systematic increase in the bulk flow velocity ($\sim 40\,\mathrm{km\,s^{-1}}$) from the low-latitude edge of the polar hole to $\pm 80.2^\circ$ (Phillips et al. 1996). The relative uniformity of most bulk flow parameters is graphically illustrated in Fig. 3, which shows the run of solar wind density and velocity measured by Ulysses during its rapid traverse between -80.2° and $+80.2^\circ$ heliographic latitude (from Phillips et al. 1995c). Note especially the very narrow range of scaled density values observed at latitudes poleward of $\pm 60^\circ$ relative to that observed below $\pm 20^\circ$. The same behavior is also evident in the run of helium abundances shown in Fig. 1. This fact was noted previously (Feldman et al. 1976b, 1977; Bame et al. 1977) and interpreted to imply that the high-speed solar wind is a fundamental, structure-free state of the solar corona. Although most other (unscaled) bulk flow parameters were observed to change along the Ulysses trajectory, these changes have been shown to result from variations in the heliocentric radial distance of the spacecraft, rather than its heliographic latitude. It therefore makes sense to use a portion of the Ulysses data measured at high latitudes to define the flow state of the high-speed solar wind as a distinct, but very special (because of its structure-free simplicity) class of coronal expansion states. For this purpose, we choose data measured poleward of $\pm 60^\circ$, which corresponds to heliocentric distances of Ulysses between 1.60 and 3.26 AU. This choice has the further virtue of fitting within a volume of space that supports a relatively constant expansion factor (see Fig. 2).

Table 1. Bulk flow parameters of the high latitude solar wind

Parameter	Mean	Median	5% level	95% level
$N_p\,R^2(\,cm^{-3})$	2.47	2.42	1.82	3.26
V_{sw} (km s^{-1})	773	774	729	812
$T_p(10^5\,K)$	1.86	1.84	1.39	2.42
$T_e(10^5\,K)$	0.844	0.779	0.565	1.222
T_α/T_p	4.76	4.73	3.98	5.61
N_α/N_p	0.0444	0.0439	0.0330	0.0574
$\Sigma(N_i\,V_i\,m_i\,R^2)(\times 10^8$AMU $cm^{-2}\,s^{-1})$	2.28	2.21	1.69	3.08
$\Sigma(N_i\,V_i^2\,m_i\,R^2)(\times 10^{16}$AMU $cm^{-1}\,s^{-1})$	1.73	1.71	1.28	2.24
$\Sigma(0.5N_i\,m_i\,V_i^3\,R^2)(\,ergs\,cm^{-2}\,s^{-1})$	1.12	1.11	0.81	1.47
Kin. + grav. energy flux (ergs $cm^{-2}\,s^{-1}$)	1.83	1.81	1.35	2.37
Heliodistance R (AU) R_{max} = 3.26 AU, R_{min} = 1.60 AU)	2.24	2.21	1.66	2.90

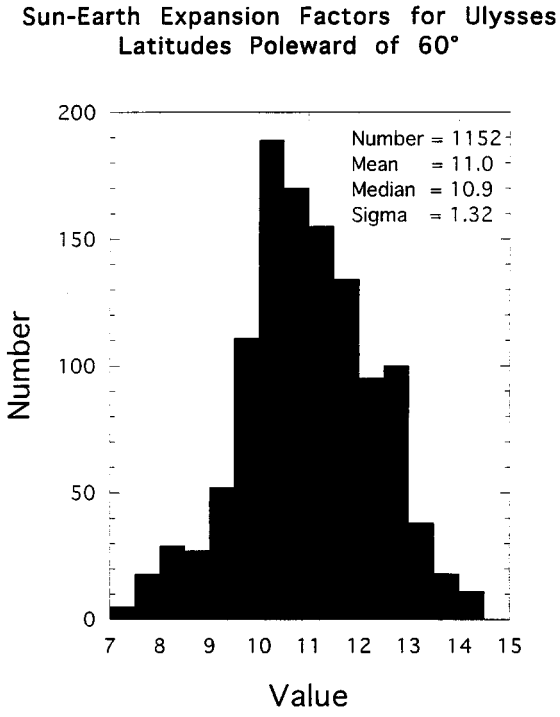

Fig. 2. Coronal expansion factors using the current-free, source-surface model described in the text for the spread of magnetic field lines at the base of solar wind flows at Ulysses when it was poleward of ±60° heliographic latitude

A selection of bulk flow parameters averaged over these parts of the Ulysses orbit is collected in Table 1. All measurements made within this latitude range were included with the exception of one CME disturbance (including the foreshocks of both forward and reverse shocks that were observed to bound the ejecta plasma), which was encountered near −61° in April 1994. The resultant set contained 71,911 hourly averages. Statistical properties of all parameters were calculated from the data as measured, with the exception that the density and its derivative parameters were scaled to 1 AU. An R^{-2} scaling law was used for this purpose, in accordance with results published separately (Feldman et al. 1996).

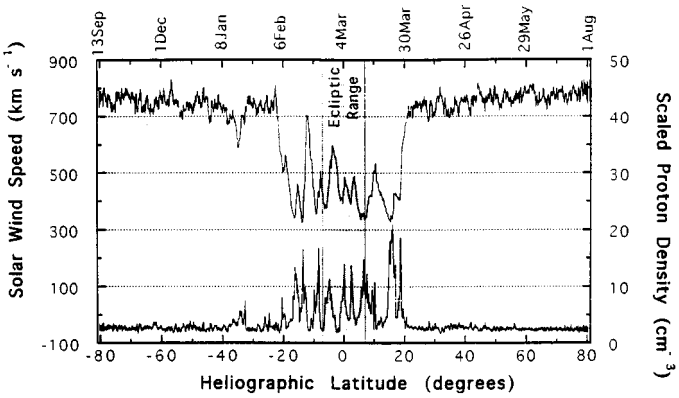

Fig. 3. Hourly averages of the solar wind bulk flow speed (upper trace) and Proton density (scaled to 1 AU, lower trace) during the rapid latitude scan of Ulysses from −80° to +80° heliographic latitude

Several facts deserve special note. A detailed comparison between the means of solar wind mass flux, momentum flux, kinetic energy flux, and total energy flux given in Table 1, rows 7 through 10, with those of the high-speed solar wind as measured in the ecliptic plane (Feldman et al. 1976b, 1977; Schwenn 1991), show excellent agreement. Whereas the scaled Ulysses high-latitude mass flux is $2.28 \times 10^8\,cm^{-2}s^{-1}$, that in the ecliptic plane at 1 AU was $2.7 \pm 0.4 \times 10^8\,cm^{-2}s^{-1}$. In addition, the summed kinetic and gravitational energy flux observed by Ulysses was $1.8\,ergs\,cm^{-2}s^{-1}$ compared to $2.0 \pm 0.22\,ergs\,cm^{-2}s^{-1}$ observed by IMP in Earth orbit. When scaled to $1R_s$ using an expansion factor of 11, these values translate to a mass flux of $1.2 \times 10^{14}\,cm^{-2}s^{-1}$, a momentum flux of $1.5 \times 10^{-2}\,g\,cm^{-1}s^{-1}$, a kinetic energy flux of $5.7 \times 10^5\,erg\,cm^{-2}s^{-1}$, and a kinetic plus gravitational energy flux (which provide the dominant contribution to the total solar wind energy flux) of $9.2 \times 10^5\,erg\,cm^{-2}s^{-1}$.

Although the proton and electron temperatures measured by Ulysses between 1.6 and 3.2 AU are less than those measured at 1 AU, the differences are consistent with their measured radial gradients (Feldman et al. 1996). Of interest for our later discus-

sion, though, is to note that the proton temperature is considerably larger (by a factor of 2.4) than the electron temperature. We also note that the ratio of alpha-particle to proton temperatures is 4.8, very close to that expected if ion temperatures scale as the ion mass. It is somewhat lower than that measured by IMP at Earth, 6.2 ± 1.3 (Feldman et al. 1977).

2.4. Shapes of ion velocity distributions

Radial projections of ion velocity distribution functions were plotted routinely throughout the entire Ulysses mission. A scan over the high-latitude portion of these data shows the sporadic occurrence of non-Maxwellian proton distributions. These are characterized by a pronounced high-energy enhancement. In contrast, the alpha-particle distributions were simple Maxwellians. Times of the largest suprathermal proton enhancements occur when the direction of the electron heat flux (and hence that of the magnetic field vector) is closest to radial. These enhancements are most pronounced at the smallest heliocentric distances. If interpreted as a relative streaming between two distinct but unresolved proton components, their relative streaming velocity then decreases with increasing heliocentric distance. A similiar decrease is also observed for the velocity difference between alpha particles and protons in the high-latitude solar wind (Neugebauer et al. 1996).

Representative examples of ion velocity distributions are shown in Fig. 4 by the vertically-stacked plot of ion energy-per-charge (E/Q) count-rate distributions measured between 1200 and 2400 UT on 17 December, 1994. Ulysses was at a latitude of -52.1° at 1.64 AU at this time. The bold-faced traces in the figure give the search-mode count rates of the Ulysses solar wind experiment (which include all E/Q voltage levels of the ion analyzer- plate power supply), and the light-shaded traces give those of the track mode data cycle (which restricts the E/Q levels to those that optimally cover the proton (low-energy column of count-rate maxima) and alpha-particle (high- energy column of count-rate maxima) peaks). Close inspection of the proton distributions reveals a pronounced high-energy enhancement superimposed on a lower energy peak that appears and disappears throughout the 12-hour period. When only a single proton peak is present, it appears at a higher E/Q level, centered at that of the pronounced high-energy enhancements of neighboring spectra. In contrast, the alpha-particle distributions show only a single peak at an E/Q level that remains constant throughout the 12-hour period. Both the secondary proton component and the total alpha-particle population therefore appear to stream faster than that of the primary proton component. This configuration is observed to occur continuously throughout the high-speed solar wind between 0.3 and 1 AU (Feldman et al. 1976a, 1993; Marsch et al. 1982a,b). A survey of all Ulysses high-latitude ion data shows this behavior to be universally observed.

Two examples of high-speed non-Maxwellian proton velocity distributions measured on 22 March, 1973 at 1 AU that demonstrate consistency with our interpretation of these distributions in terms of a double-streaming proton configuration, are reproduced from Feldman et al. (1976a) in Fig. 5. Whereas the top two panels give one-dimensional (1-D) projections of the proton velocity distribution function, those on the bottom give two-dimensional (2-D) contours of the corresponding distribution functions. Also superimposed on the 1-D plots are the radial projections of a model containing two, relatively convecting bi-Maxwellian functions. Inspection shows the fits to be excellent. The fraction of the total proton density carried by the higher energy component is 0.39 and 0.32 for the left- and right-hand distributions, respectively, and both secondary (higher-energy) components are traveling faster than the primary (lower-energy) components by about the local Alfvén speed. This behavior generally obtains throughout the high-speed solar wind, although the fractional density of the secondary component is lower on average, amounting to about 25% of the total.

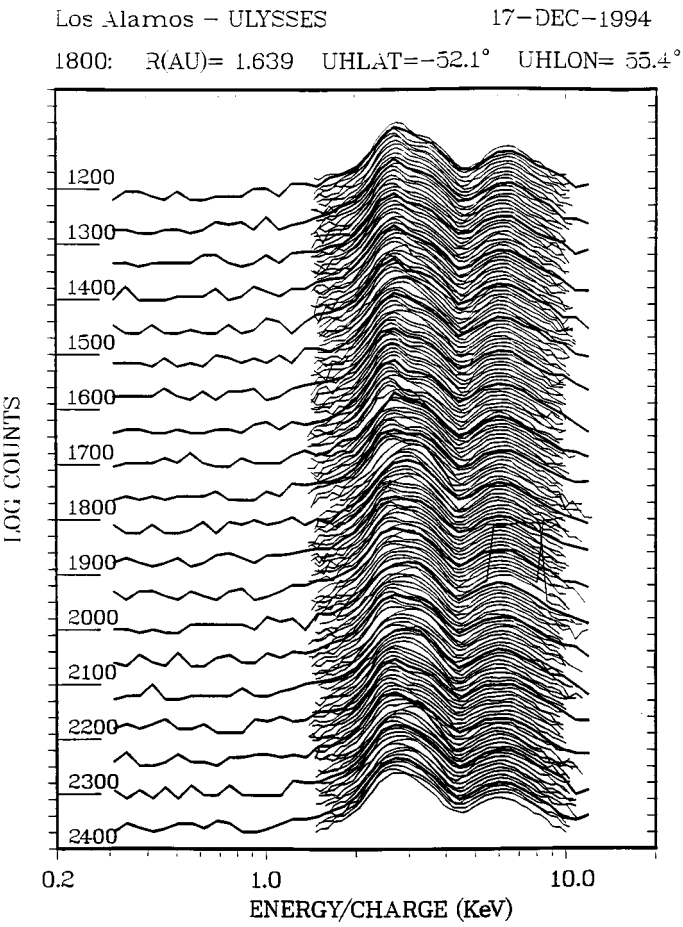

Fig. 4. Histogram of hourly averages of the solar wind helium abundance observed by Ulysses when it was poleward of $\pm 60^\circ$ heliographic latitude

2.5. The abundance of helium

One-hour averages of the solar wind helium abundance, [He], are shown in the bottom trace of both panels of Fig. 1. Inspection shows it to be quite variable when the solar wind bulk speed is low, and relatively constant when the speed is high. Indeed, the only departures from a narrow range of helium abundances

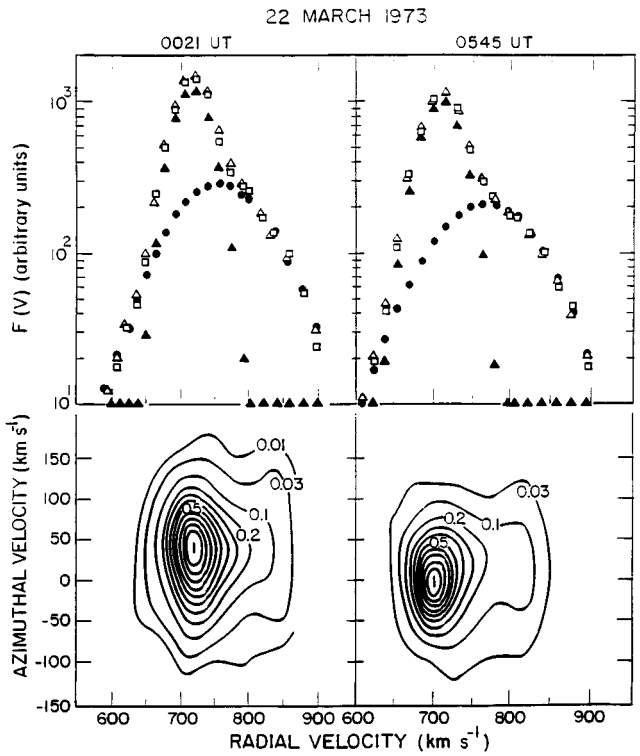

Fig. 5. A stacked plot of Ulysses ion energy-per-charge count-rate spectra measured at a heliocentric radial distance of 1.6 AU and at a heliographic latitude of -52.1° on 17 December, 1994

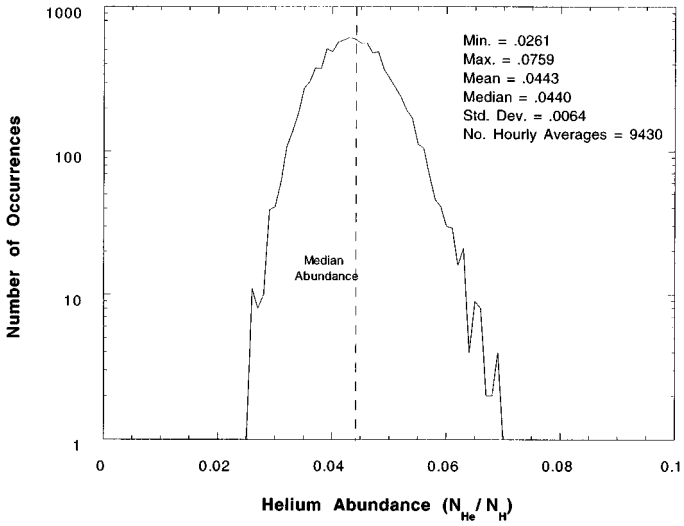

Fig. 6. Two examples of ion velocity distributions measured by IMP 7 in Earth orbit on 22 March, 1973. The top panels show 1-D projections of fits to two 2-D solar wind proton velocity distributions while the bottom panels show 2-D contours of the same distributions (from Feldman et al. 1976b). The model chosen for the fits uses a superposition of two, relatively convecting bi- Maxwellian components

were encountered at low speeds, seen in Fig. 1 as short-term occurrences of both high and low values, generally associated either with CMEs or with streamer-belt plasma (Barraclough et al. 1996).

A histogram of hourly averages of [He] for that portion of all Ulysses data measured poleward of $\pm 60^\circ$ is presented in Fig. 6. Data from the CME interval in April 1994 (the only CME observed poleward of $\pm 60^\circ$) were not included. The same exclusionary criterion was also chosen for the bulk parameter averages presented in Table 1. Inspection of Fig. 6 shows a single, nearly symmetric (on a log-linear display) peak that has a mean of 4.4% and a full-width at half maximum of about 0.64% . This level of variation is very low for general solar wind flow conditions (Bame et al. 1977; Feldman et al. 1977), but is consistent with that observed in the high- speed solar wind in the ecliptic at 1 AU ([He]=4.8% , Feldman et al. 1977; [He]=3.6% , Schwenn 1991; [He]=4.5% , Ogilvie et al. 1989). A histogram of [He] for all Ulysses high-speed data measured poleward of $\pm 40^\circ$ (with CME events excluded) measured prior to August, 1995 was presented in Feldman et al. (1996), showing closely similar results. A point that is especially important, which we will return to inSect. 3, is that the mean hourly-averaged value of [He] from Fig. 6 is about a factor of 2 less than that of the solar convection zone inferred from helioseismic data (e.g., Kosovichev 1995, and references therein). Furthermore, the maximum hourly-averaged value of [He] in the high-latitude wind, 7.6% , is less than the minimum inferred helium abundance in the solar convection zone, 8.2% .

3. Comparison with remote-sensing observations

3.1. Overview

Much is known about conditions in coronal holes from remote sensing observations. An explosion of new data, which spawned a corresponding explosion of new models of the structure of the chromosphere-corona transition region and low corona, was generated by the Skylab mission in the mid-to- early 1970s (see summary of early results in "Coronal Holes and High Speed Wind Streams", Zirker, ed., 1977). A continuous succession of new experiments, and correspondingly more refined models of the extended solar atmosphere in coronal holes, has appeared ever since. A good summary of its basic structure was given in Withbroe and Noyes (1977), and summaries of later ideas were given in Withbroe (1988) and Habbal (1992a). According to the presently accepted paradigm, virtually all magnetic field lines that connect the photosphere to interplanetary space in coronal holes originate in concentrated magnetic flux bundles that cluster at the margins of supergranular flow patterns in the photosphere, defined by the chromospheric network. These field concentrations quickly expand with altitude to fill the interior portions of the supergranules above a thin transition zone that is marked by an extremely large temperature gradient (Gabriel 1976). The altitude above the photosphere of the resultant horizontal canopy of magnetic field lines that spread from the flux bundles is less than about 1000 km. Plasma conditions in the corona above this transition zone are much more uniform, and to zeroth order appear to be constant in both space and time. Nev-

ertheless, time variations in the low corona have been observed (see, e.g., Habbal, 1992a,b, and references therein), which become more prominent at lower temperatures, at lower altitudes above the photosphere (see, e.g., Dere, 1994, and references therein). Although many plausible suggestions have been proposed and theoretically developed to explain the origin of a million-degree corona within holes at the base of the high-speed solar wind, we have as yet no clear understanding of the chain of physical mechanisms that support its existence.

3.2. Transient events in coronal holes

A common theme to all observations presented in Sect. 2 was the very low variance of all scaled parameters (including [He] = N_{He}/N_H and T_α/T_p) in the high-latitude solar wind. Yet, remote sensing observations of the chromosphere-corona transition region and the low corona in coronal holes (which are magnetically open to interplanetary space) reveal a multitude of transient events that induce large changes in plasma conditions from its average state near the Sun. Examples include spicules, macrospicules, EUV explosive events, bright-point flares, polar plumes, X-ray jets, and H α surges. Each of these events produces strong disturbances that reach the base of the solar wind and so should induce some corresponding change in the overlying flow. Yet no significant variations were observed by Ulysses during more than 650 days in the high-latitude wind poleward of $\pm 40°$. Additionally, a search for such effects in Helios data revealed only marginally detectable pressure-balanced, variable speed flow structures between 0.3 and 1 AU (Thieme et al. 1989). Why are more pronounced variations not more prevalent? Perhaps they occur so infrequently that their effects were simply missed.

This possibility is addressed in Table 2 by collecting data that summarize the properties of two of the seven types of transient events just listed, spicules and EUV explosive events (see, e.g., Beckers 1972, and Dere 1994, respectively). The third data column in Table II supplements extrapolations of Ulysses data presented in Sect. 2 with: 1) spatial scales of possible bulk- flow variability from Helios data (that of a supergranule, Thieme et al. 1989), and 2) characteristics of possible jet-like events at the coronal base that are needed to explain the shapes of proton and helium velocity distributions in the high-speed solar wind (Feldman et al. 1993; Feldman & Marsch 1996). These data are consistent with the observed replacement rate of all open magnetic field lines from reconnection to granular-sized magnetic bipoles that are swept into the chromospheric network after emerging through the photosphere in the interiors of supergranules (Livi et al. 1985; Zirin 1987; Martin 1988).

Spicules are upward-going, relatively low-speed ($\sim 25\,\mathrm{km\,s^{-1}}$) jets of chromospheric material that penetrate into the low corona to altitudes up to 9000 km above the photosphere. They occur in the chromospheric network of strong magnetic fields that bound supergranules, have a spatial scale of ~ 800 km, and a time scale of $\sim 300\,s$. Although they carry an energy flux density, $5 \times 10^3\,\mathrm{ergs\,cm^{-2}s^{-1}}$, which is insignificant relative to that carried off by the overlying solar wind, $9.2 \times 10^5\,\mathrm{ergs\,cm^{-2}s^{-1}}$, and conducted downward to the chromosphere, $\sim 1 \times 10^5\,\mathrm{erg\,cm^{-2}s^{-1}}$, they transport enough mass flux density to supply 10 times that carried away from the corona by the solar wind (compare the first and third data columns in Table 2). Most importantly, they occur on every magnetic field line that connects the photosphere to interplanetary space at a rate of 130 per day. The effects of these events on the solar wind flow, if they exist, could therefore not have been missed by Ulysses (or by any of the many previous missions that have been used to observe the solar wind).

The same conclusion holds for EUV explosive events. These events are also jets of plasma, but that are observed to start at altitudes below $\sim$ 2000 km in the transition region and extend to heights above the photosphere greater than 40,000 km. They have temperatures of $\sim 10^5$ K and a range of velocities that fill a continuum with end point of $\sim 100\,\mathrm{km\,s^{-1}}$. They occur at the margins of the chromospheric network within supergranules, have a spatial scale of $\sim$ 1500 km, and a time scale of $\sim$ 60 s. Statistics for their observed occurrence rate (Dere 1994) yield a birthrate of between 0.5 and $1 \times 10^{-20}\,\mathrm{cm^{-2}s^{-1}}$. Adopting the lower value of their estimated birthrate and the transition-region model of Gabriel (1976), the transient jets generated by these events should affect plasma conditions on every field line that threads through the base of the solar wind at a rate of at least 7.6 times per day.

We note by comparing the data in columns 2 and 3 in Table 2 that the various data sets do not support a single, simple interpretation. The total mass and energy flux that explosive events are observed to deliver to the corona is far below that needed to supply all losses to the solar wind. Yet their rate of occurrence is far higher than that needed to account for the rate at which all open field lines are replaced through reconnection with the magnetic flux in disappearing magnetic bipoles seen in photospheric magnetograms (Martin 1988). However, the rate of energy dissipation in these disappearing events is sufficient to support all energy losses of the corona, including that of the solar wind (Parker 1991, 1992).

3.3. The coronal helium abundance

The foregoing estimates of the rates of a subset of the total number of solar transient events, observed to occur between the photosphere and the base of the solar wind, is difficult to reconcile with the observed constancy of the helium abundance in the high-speed solar wind. The source of this difficulty is that the value of solar wind [He], 4.4% , is considerably below that inferred from helioseismic data to exist throughout the solar convection zone, $\sim$ 8.2% (see, e.g., Guzik & Cox 1993; Kosovichev, 1995, and references therein). It is also more than a factor of 2 below our best estimate of the cosmic helium abundance, $\sim$ 9.6% (e.g., Iben 1969, and references therein), which presumably constituted the helium abundance in the primordial solar nebula (e.g., Bahcall & Pinsonneault 1992, and references therein). This discrepancy has been explained as due to fractionation driven by thermal and gravitational diffusion in the region between the chromosphere and the low corona (see,

Table 2. Properties of spicules and explosive events

Parameter	Spicules	Explosive events	Base polar corona
Velocity ($km\,s^{-1}$)	25	100	800
Mass flux density ($cm^{-2}s^{-1}$)	1×10^{15}	7.4×10^{11}	1.2×10^{14}
Energy flux density($ergs\,cm^{-2}s^{-1}$)	5×10^{3}	2×10^{4}	9.2×10^{5}
Spatial scale (km)	800	1500	3×10^{4}
Time scale (s)	300	60	1×10^{5}
Height (km)	< 9000	> 2000	$> 10^{6}$
Birthrate ($km^{-2}\,s^{-1}$)	3×10^{-9}	0.5×10^{-10}	1.6×10^{-14}
Replenishment rate (day^{-1})	130	7.6	~ 1

e.g., von Steiger & Geiss 1989; Hansteen et al. 1993). However, if this explanation is correct, the diffusion process should produce significant spatial gradients in the helium abundance of the chromosphere- corona transition region. Why then, are these gradients not reflected in the high-speed solar wind as discrete temporal variations of [He] (both low and high) in response to the multitude of transient events that mix all layers of the atmosphere above the photosphere on a time scale short compared to the solar wind expansion time? No such discrete helium variation events were observed by Ulysses in more than 650 days poleward of $\pm 40^{\circ}$ in the high-latitude solar wind. Nor are any other first-ionization-potential fractionation effects detected in this flow, although they occur prominently in the low-speed solar wind at lower latitudes (von Steiger et al. 1995). Both results are reinforced by the absence of enhanced helium abundance within six CME events that were encountered by Ulysses at high heliographic latitudes (Barraclough et al. 1996), even though such abundance enhancements are often used as one of the defining characteristics of CMEs at low latitudes (see, e.g., Gosling 1990, and references therein).

3.4. Other relevant remote-sensing data

Although no existing remote-sensing data set has been sufficient to unambiguously identify the mechanisms that heat the corona and accelerate the solar wind, it is still possible, by assembling a composite data set, to strengthen the arguments that favor one or more guesses. We adopt this philosophy in the hopes of gaining insight. Starting from the low corona and proceeding outward, we note first that spectral shapes of the Ly α line measured by Spartan 201 at $1.8\,r_s$ can be interpreted in terms of a two-component gas mixture (Kohl et al. 1995). Whereas the dominant component has a temperature of 1.6×10^{6} K, the minor component can be characterized as having a random speed perpendicular to B (assumed to be radial) of about $300\,km\,s^{-1}$. If contributions to the continuum are neglected, and no relative correction is made for Doppler dimming (consistent with the assumption that both components have equal flow speeds at $1.8\,R_s$), then the fractional abundance of the minor component relative to the total neutral hydrogen gas density amounts to about 60% .

Comparison of the 1 AU scaled solar wind mass flux measured by Ulysses ($2.28 \times 10^{8}\,cm^{-2}s^{-1}$), with the density of the polar corona at $5.5\,R_s$ measured by the white-light coronagraph aboard Spartan 201 ($4 \times 10^{3}\,cm^{-3}$, see, e.g., Habbal et al. 1995), allows an estimate of the radial extent of the solar wind acceleration region in the high-latitude solar wind. Combining the flow tube divergences calculated using the combined source-surface and current-sheet model of Wang and Sheeley (1995) with conservation of mass flux yields $980\,km\,s^{-1}$ for the speed of the solar wind at $5.5\,R_s$. This speed is larger than that measured by Ulysses, $773\,km\,s^{-1}$, between 1.6 and 3.26 AU. We therefore conclude that all acceleration of the solar wind must occur at radial distances less than $5.5\,R_s$.

IPS data measured at a closest approach distance of $5\,R_s$ in a coronal hole provide two additional valuable clues. The first is detection of a pronounced enhancement in the structure functions of electron density irregularities, which have scales that range between about 0.1 and 10 proton gyroradii (Coles et al. 1991; Grall et al. 1996). These irregularities are strongly anisotropic, having radially aligned axial ratios amounting to 10:1. A second observation is that the patterns of these irregularities move with apparent radial speeds that range between 400 and $1280\,km\,s^{-1}$ (Klinglesmith et al. 1995). As we will discuss in the next section, both these observations are consistent with (but do not conclusively prove) the existence of an ensemble of filamentary plasma jets that are sufficiently structured to relax through generation of a drift- wave instability that results in electrostatic waves having k-vectors oriented perpendicular to B (see discussion in chapter 4 of Gary 1993). We also note that the foregoing IPS speed range brackets the Ulysses bulk flow speed projected to $5.5\,R_s$.

Several characteristics of the high-speed solar wind also provide constraints (although again not definitive) on the mechanisms that shape the solar corona. As mentioned earlier, three such characteristics are; 1) Velocity unresolved proton double streams, accompanied by a single alpha-particle beam, are continuously present. Both the alpha-particle and the secondary proton beams travel at speeds that are faster than that of the primary protons by about the local Alfvén speed. 2) The proton temperature is on average a factor of 2.4 times higher than that of the electrons. And 3), the abundance of helium is relatively constant at an average level that is about a factor of two lower than that in the solar convection zone. Although all of these characteristics have been noted previously in the ecliptic plane (see, e.g., Feldman et al. 1977; Schwenn 1991; Feldman & Marsch

1996), their observation by Ulysses over a more than 650-day period in the high-latitude wind suggests that they are intrinsic properties of the high-speed solar wind and not a product of the boundary layer between coronal holes and the streamer belt.

A last characteristic that may have a bearing on coronal structure is the continuous presence of a field of large-amplitude Alfvén waves (Balogh et al. 1995). This feature has also been known for some time (see, e.g., Belcher & Davis 1971). We wish to note though, that the length scales carrying most of the wave energy flux density are large compared to coronal scale distances. When viewed as a time series of data, the "Oscillations" in B are not periodic, but seem to swing rapidly from one angular extreme to another over a continuum of time scales (Belcher & Davis 1971).

4. Discussion and conclusions

4.1. Self-consistent model of the corona

All of the foregoing results can be understood if the entire solar atmosphere above the photosphere is thoroughly mixed along all magnetically-aligned flow tubes by convective transients on a time scale shorter than diffusion can gravitationally settle helium to lower altitudes. Indeed, theory predicts a diffusion time in the low corona of the order of one day (Hansteen et al. 1993), yet spicules occur at a rate of about 130 times per day, and explosive events occur at a rate of more than 7.6 times per day, on every field line that connects the photosphere to interplanetary space. Of course macrospicules, bright-point flares, polar plumes, X-ray jets, and H α surges should also add to the total atmospheric mixing rate, thereby strengthening our conclusion. This conclusion, though, raises other questions. What is the role of atmospheric mixing events in determining the structure of the corona and in accelerating the solar wind? How do we reconcile the fact that EUV explosive events occur at a rate about ten times higher than the occurrence rate of magnetic flux disappearing events, while at the same time, explosive events are observed to deliver an energy flux to the atmosphere that is about twenty times lower than that delivered by the disappearing flux events? Nevertheless, both types of events are inferred to be driven by magnetic reconnection of newly emerged magnetic bipoles with field at the margins of the chromospheric network, and should therefore be related. And finally, how do we reconcile the difference (close to a factor of two) in helium abundance between a well mixed convection zone and a well mixed atmosphere above the photosphere?

We, of course, do not know the answers to these questions and so can only speculate at this time. The data suggest, though, that plasma jets from explosive-type events figure importantly in defining the structure of the low corona because their effects are observed in the overlying solar wind. Indeed, the preferred interpretation of the non-Maxwellian proton distributions observed throughout the high-speed solar wind (see also Feldman et al. 1993; Feldman & Marsch 1996) is in terms of an ensemble of coronal plasma jets. Other explanations in terms of wave damping at low heliocentric distances and suprathermal runaway have been proposed. But, whereas the first requires a strong source of coherent waves in the corona, which is not very likely, the second predicts an enhancement in the suprathermal portions of proton distributions that become more pronounced with increasing heliocentric distance (Livi & Marsch 1987). This prediction runs counter to observations, as the interpenetrating proton beams that comprise the high-speed solar wind become less resolved in velocity as the heliocentric radial distance increases (Marsch, et al. 1982a). In addition, measurements reveal a resolved secondary peak in proton distrubution functions at 0.3 AU (Marsch et al. 1982a), a heliocentric distance much less than that consistent with suprathermal runaway (Livi & Marsch 1987). A more conclusive confirmation of a plasma configuration in coronal holes that consists of an ensemble of filamentary plasma jets has been found recently in IPS observations at heliocentric distances between 5 and 10 R_s (Klinglesmith et al. 1995). These data are consistent with patterns of density fluctuations that appear to propagate radially outward at speeds that range between 400 and 1280 km s^{-1} for a given view direction along the line of sight. We note that this continuum of speeds is qualitatively similar to that observed in the transition region, but occurs over a speed range that is a factor of ten times higher. Could both observations relate to the same physical reconnection events in the chromosphere-corona transition region but stem from acceleration at different altitudes? Indeed, the global magnetic configuration suggested to explain such an event (Dere 1992) supports this interpretation, as illustrated in Fig. 7 (constructed to explain the double proton streams in the high-speed solar wind, Feldman et al. 1993). Plasma simulations of this class of magnetic configuration (first suggested by Heyvaerts et al. 1977, to expain a class of solar flares) have been shown to reproduce much of the structural morphology of anemone-type X-ray jets observed by Yohkoh (Yokoyama & Shibata 1995), which also shares the same magnetic topology.

In this picture, magnetic reconnection occurs at a current sheet that forms between an emerging bipolar magnetic region and the underside of the magnetic canopy produced by upward expansion of the tight magnetic flux bundles that form in the chromospheric network. The site of this reconnection is shown by the black rectangle in Fig. 7. After severence, the nonpotential magnetic fields on either side of the reconnection site relax to form two oppositely directed jets that are bounded by four 2-D plasma sheets that are slow-mode shocks (see Petchek 1964). Concentrating on the jet directed toward the upper left, plasma is accelerated at both shock surfaces by $J \times B$ forces from two distinct sources. That from the lower left contains cool and relatively high density chromospheric material, and that from the upper right contains hot and relatively low density coronal material. Conservation of transverse momentum flux across these shocks implies acceleration to speeds in the jets that is close to, but less than, the upstream Alfvén speed (depending on how close the shock is to a cutoff configuration, see, e.g., the analysis of a magnetic reconnection event in the Earth's magnetotail detailed in Feldman et al. 1987). The Alfvén speed is highest in the low corona (approaching 1500 km s^{-1}, see models in Withbroe 1988) because of its relatively low den-

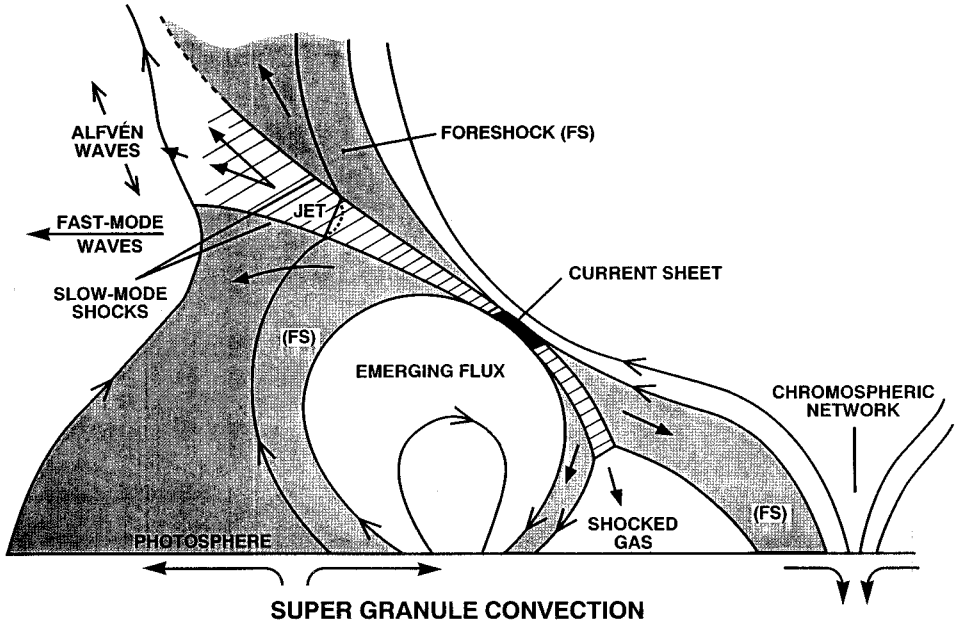

Fig. 7. A cartoon illustrating a plasma configuration in the chromosphere-corona transition region that may be responsible for a host of transient-related phenomena inferred from remote-sensing data. See the text for an explanation

sity, and is lowest in the chromosphere because of its relatively high density. This speed increases continuously with increasing height at all altitudes along both 2-D shock surfaces in Fig. 7. We therefore expect this type of configuration to produce a range of speeds within the jets depending on where along each of the slow-shock sheets the plasma was accelerated into the jets. In general, jet material coming from the cooler chromosphere and transition-region will end up over a range of relatively slow speeds (and resultant lower temperatures) in the jet, and that from the hotter corona will end up over a range of relatively fast speeds (and resultant higher temperatures). This expectation is consistent with the results of simulations of a combined X-ray jet and H α surge by Yokoyama and Shibata (1995), and with both the EUV and IPS observations discussed above.

The foregoing model of coronal structure as composed of an ensemble of relatively high-speed jets, provides a ready explanation of why the jets observed in the EUV at lower altitudes account for only a small fraction of the mass and energy flux of the high-speed solar wind. The brightest emission will come from the region of highest density (because emission measure is proportional to the square of the density) near the site of reconnection. This region is immersed in relatively low temperature and high density plasma having a relatively low Alfvén speed, and hence will produce a low jet speed. According to Dere (1994), the structure at this location is extremely filamentary, characterized by a volumetric fill factor of 10^{-4} . Such a structure is unstable to the generation of electrostatic drift waves (see, e.g., chapter 4 of Gary, 1993), which should cause the filaments to fill in at increasing distances from the reconnection site, thereby quickly lowering the emission rate below detection threshold. We expect the material that emits in the EUV at a temperature of $\sim 10^5$ K to comprise only that small fraction of all the jet material that flows at the lowest speeds. It is not surprising, therefore, that its mass and energy flux accounts for only a small fraction of the total flux needed to supply all losses to the overlying solar wind.

Another factor that helps explain the discrepancy between the observed low upward-going kinetic energy flux in the EUV transients can be seen by studying Fig. 7. Much of the low-speed EUV emitting plasma is propagating horizontally to the left. This material will be stopped by, and transfer much of its energy and momentum to, the plasma on the open field lines that connect to the chromospheric network on the opposite margin of the surpergranule. The net result should be the generation of fast-mode waves that propagate into, and heat the coronal plasma in neighboring flow tubes, and the generation of Alfvén waves that propagate both downward to the chromosphere (where they are absorbed, and their energy reradiated) and upward into the solar wind (where they provide an extended source of energy and momentum flux to the solar wind). Indeed, this interaction provides a natural explanation for the stochastic appearance of large-amplitude, long-period Alfvén waves in the solar wind (Belcher & Davis 1971). It is also consistent with the fact that extrapolation to the coronal base of the energy flux of Alfvén waves observed between 0.3 and 1 AU yields a value that amounts to at most 40% (Roberts, 1989), but most probably only a few percent (Smith et al. 1995), of that required to drive the entire high-speed solar wind. While this fraction is not enough to provide the primary source for acceleration of the solar wind, it very well could be a secondary bi-product of the primary source, which in this case is the reconnection-driven plasma jets. This explanation of solar wind Alfvén waves also solves a long standing problem of extended coronal heating. Observations of the chromosphere-corona transition region are not consistent with a flux of upward propagating acoustic waves that is sufficient to supply all of the energy losses of the overlying corona (Athay & White 1978). The model of a jet-heated corona just described bypasses this problem by generating the

requisite flux of waves at the coronal base and not at lower levels, as generally assumed by all previous models.

Following the same speculative vein, the visibility of the largest portion of the jets at higher altitude (where the dominant fraction of the mass and energy flux is carried) is expected to be low, both because the jet has spread and the feeder density is low, and because the end-point speed of the jet is very high, approaching the upstream Alfvén speed at about 1500 km s^{-1}. The resultant large spread in speeds in the jet would be very difficult to recognize in EUV line-shape profiles because they would radiate in the far wings of the various coronal EUV lines and therefore lose their ion- identification wavelength property by merging into the continuum (1000 km s^{-1} at the 625 Å Mg X line corresponds to a Doppler shift of about 2 Å).

Given this basic picture of a filamentary, transient, jet-like coronal structure at the base of the high-speed solar wind, a host of phenomena should occur at higher altitudes. These were shown to be consistent with solar wind measurements at large heliocentric distances (see the discussion in Feldman et al. 1993). For example, heating and acceleration of plasma by slow-mode, reconnection-generated shocks results in an ion temperature that is much higher than the electron temperature, as observed in the terrestrial magnetosphere (in the one reconnection event studied in detail, shocked protons were hotter than the electrons in the geomagnetic tail by a factor of 3.4, Feldman et al. 1987). As seen in Table 1, this condition obtains in the high- speed solar wind (see also Feldman et al. 1976b). The upward-going portion of the jet will also interact with the slower-moving ambient plasma above it on the same field line through Coulomb friction, thereby further enhancing the temperature difference between ions and electrons (because most of the energy flux carried by the jet resides in the bulk convection of the ions). If this basic picture of a transient , reconnection-heated corona is correct, then the difference between the observed rate of EUV explosive events and magnetic flux disappearing events implies either a fragmentary, multistep flux annihilation process at the margins of supergranules, or a threshold effect in identifying magnetic bipoles in magnetograms (the threshold used for the flux disappearing events was 20 G, Martin 1987).

In conclusion, the sum total of all remote-sensing observations appear to be consistent with (although do not definitively require) a coronal structure that is fundamentally temporally and spatially dependent, consisting of sporadic jets of plasma having relatively high density and high speed, coursing through a generally low density, low speed, and low temperature ambient corona. If these inferences are correct, then conditions within a coronal hole close to the Sun should consist of an ensemble of solar wind flow states ranging from relatively slow ($\sim$ 400 km s^{-1}) to relatively fast ($\sim$ 1300 km s^{-1}) speeds. The slow flow state may have an enhanced helium abundance and a depressed alpha-particle flow speed at the coronal base, and the fast flow state may have ion velocity distributions reflecting multiple beams of interpenetrating ion components. Both states may contain occasional bursts of relatively large-amplitude hydromagnetic waves covering a broad range of wave numbers up to the inverse proton gyroradius. They may also contain bursts of suprathermal and energetic ions and electrons associated with filamentary-scale magnetic reconnection below the coronal base. The cadence of such events should be consistent with the cadence of granule-sized reconnection events (EUV explosive events, see, e.g., Dere 1994, and references therein) observed in the chromosphere-corona transition region.

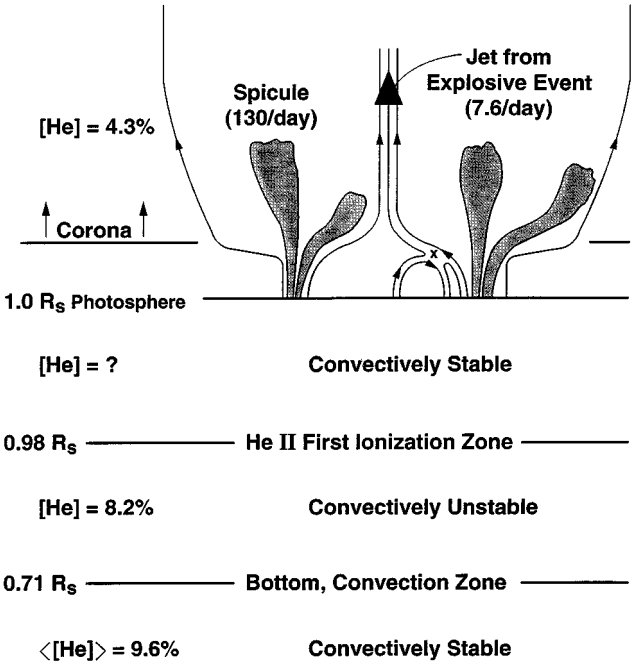

Fig. 8. A cartoon illustrating two of the many transient events known to occur above the photosphere and their relation to the different zones of helium abundances inferred from helioseismic data. See the text for an explanation

4.2. Model of the solar helium abundance

The difference noted previously between the helium abundance above and below the photosphere is a zeroth-order effect and needs to be addressed. A visual summary of the radial structure of helium abundances inferred from helioseismology and solar wind measurements, is shown in Fig. 8. Four zones are delineated. Arguments that support a uniform abundance of 4.4% on average above the photosphere were presented earlier in this paper. The combination of analyses of helioseismic data (see, e.g., Antia & Basu 1994; Kosovichev 1995, and references therein) and extensive modeling of the Sun (see, e.g., Bahcall & Pinsonneault 1992; Guzik & Cox 1993, and references therein) have provided a self-consistent picture of the run of helium abundance with depths below the bottom of the helium II first ionization zone, $\sim$ 0.98 R_S. The helium abundance decreases gradually from the center of the Sun outward to the bottom of the convection zone due partly to the production of helium in the core during hydrogen burning, and to a small amount of gravitational settling. Gas between 0.71 R_S (which marks the bottom of the convection zone), and $\sim$ 0.98 R_S (which marks the location of the bottom of the He II first ionization zone), is

convectively unstable. This condition has spawned several models of the equation of state that is relevant to this region, which has been combined with a subset of helioseismic frequencies to determine the change in adiabatic index of the gas across this zone and, in turn, its mean molecular weight. Resultant helium abundances range between 0.078 and 0.086 by number at the height of the He II first ionization zone (Kosovichev, 1995). Solar gas cools to low enough temperatures above this height that an ever larger fraction of helium becomes neutral, thereby lowering the opacity of the gas enough that its temperature gradient falls below the threshold for convective instability. The zone of gas extending from $\sim$ 10 000 km below the photosphere to the photosphere is therefore convectively stable. Because of the proximity to the photosphere, the properties of this layer are difficult to model and no estimates of [He] from helioseismic data have been made. We have therefore inserted a question mark next to [He] in this layer in Fig. 8. A temporary (very speculative) solution to our problem is to identify this layer as the place where thermal/gravitational diffusion (or some other process) causes a reduction in [He] from the 8.2% that exists throughout the solar convection zone to the 4.4% that obtains above the base of spicule formation.

Acknowledgements. We owe much thanks to B. Goldstein for his exceptional effort in leading the Ulysses ion data-reduction effort. We have also benefited from many insightful conversations with J. Gosling, S.P. Gary, W. Coles, S. Habbal, and L. Strachan, to place the Ulysses data into its proper physical context. Work at Los Alamos was performed under the auspices of the U.S. Department of Energy with financial support from NASA.

References

Antia H.M., Basu S., 1994, ApJ 426, 801
Athay R.G., White O.R. 1978, ApJ 226, 1135
Axford W.I., McKenzie J.F. 1992, in: Marsch E., Schwenn R. (eds.) Solar Wind Seven. Pergamon Press, Oxford, p. 1
Bahcall J.N., Pinsonneault M.H., 1992, ApJ 395, L119
Balogh A., Smith E.J., Tsurutani B.T., et al. 1995, Science 268, 1007
Bame S.J., Asbridge J.R., Feldman W.C., Gosling J.T. 1977, J. Geophys. Res. 82, 1487
Bame S.J., McComas D.J., Barraclough B.L., et al. 1992, A&AS 92, 237
Bame S.J., Goldstein B.E., Gosling J.T., et al. 1993, Geophys. Res. Letters 20, 2323
Barraclough B.L., Gosling J.T., Phillips J.L., et al. 1996, in: Winterhalter D. (ed.) Proceedings of the Eighth International Solar Wind Conference (in press)
Beckers J.M., 1972, ARA&A 9, 73
Belcher J.W., Davis L. 1971, J. Geophys. Res. 76, 3534
Coles W.A., Lui W., Harmon J.K., Martin C.L. 1991, J. Geophys. Res. 96, 1745
Dere K.P. 1992, in : Marsch E., Schwenn R. (eds.) Solar Wind Seven Pergamon Press, Oxford p. 11
Dere K.P. 1994, Adv. Space Res. 14, 13
Feldman W.C., Marsch E. 1996, in : Jokipii J.R., Sonett C.P., Giampapa M.S., Matthews M.S. (eds) Cosmic Winds and the Heliosphere Univ. Ariz. Press, Tucson (in press)
Feldman W.C., Abraham-Shrauner B., Asbridge J.R., Bame S.J. 1976a, in : Williams D.J. (ed.) Physics of Solar Planetary Environments, Vol. 1, Amer. Geophys. Union Publ. p 413
Feldman W.C., Asbridge J.R., Bame S.J., Gosling J.T. 1976b, J. Geophys. Res. 81, 5054
Feldman W.C., Asbridge J.R., Bame S.J., Gosling J.T. 1977, in : White O.R. (ed.) The Solar Output and its Variations, Boulder:Col. Assoc. Univ. Press, p. 351
Feldman W.C., Tokar R.L., Birn J., et al. 1987, J. Geophys. Res. 92, 83
Feldman W.C., Gosling J.T., McComas D.J., Phillips J.L. 1993, J. Geophys. Res. 98, 5593
Feldman W.C., Phillips J.L., Barraclough B.L., Hammond C.M. 1996, in : Tsinganos K. (ed.) Proc. NATO ASI on Solar and Astrophysical MHD Flows (in press)
Gabriel A.H. 1976, Philos. Trans. Roy. Soc. London Ser. A 281, 339
Gary S.P. 1993, Theory of Space Plasma Microinstabilities. Cambridge Univ. Press, Cambridge
Gosling J.T. 1990, in : Russell C.T., Priest E.R., Lee L.C. (eds.) Physics of Magnetic Flux Ropes, Geophys. Monogr. Ser., Vol. 58, AGU, Washington D.C., 343
Gosling J.T., Bame S.J., Feldman W.C., et al. 1995, Geophys. Res. Letters 22, 3329
Grall R.R., Coles W.A., Klinglesmith M.T., et al. 1996, Nature (in press)
Guzik J.A., Cox A.N. 1993, ApJ. 411, 394
Habbal S.R. 1992a, Annal. Geophysic. 10, 34
Habbal S.R. 1992b, in : Marsch E., Schwenn R. (eds.) Solar Wind Seven, Pergamon Press, Oxford, p 41
Habbal S.R., Esser R., Guhathakurta M. Fisher R.R. 1995, Geophys. Res. Letters 22, 1465
Hansteen V.H., Holzer T.E., Leer E. 1993, ApJ 402, 334
Heyvaerts J., Priest E.R., Rust D.M. 1977, ApJ 216, 123
Iben I Jr. 1969, Annals of Phys. 54, 164
Klinglesmith M.T., Coles Wm.A., Grall R.R., 1995, EOS, Abstract, p F470
Kohl J.L., Gardner L.D., Strachan L., Fisher R., Guhathakurta, M. 1995, Space Sci. Rev. 72, 29
Kosovichev A.G. 1995, Adv. Space Res. 15, 95
Livi S., Marsch E. 1987, J. Geophys. Res. 92, 7255
Livi S.H.B., Wang J., Martin S.F. 1985, Aust. J. Phys. 38, 855
Marsch E., Mühlhäuser K.-H., Schwenn R., et al. 1982a, J. Geophys. Res. 87, 52
Marsch E., Mühlhäuser K.-H., Rosenbauer H. Schwenn R., Neubauer F.M. 1982b, J. Geophys. Res. 87, 35
Martin S.F. 1988, Sol. Phys. 117, 243
McKenzie J.F., Banazkiewicz M., Axford W.I. 1995., A&A 303, L45
Neugebauer M., Goldstein B.E., Smith E.J., Feldman W.C. 1996, J. Geophys. Res. sub.
Ogilvie K.W., Cjoplan M.A., Bochsler P., Geiss J. 1989, Solar Phys. 124, 167
Parker E.N. 1991, ApJ. 372 719
Parker E.N. 1992, in : Marsch E., Schwenn R. (eds.) Solar Wind Seven, Pergamon Press, Oxford p. 79
Petschek H.E., 1964, in : Ericson W. (ed.) AAS-NASA Symposium on the Physics of Solar Flares, NASA Spec. Publ. SP-50, p 425
Phillips J.L., Bame S.J., Feldman W.C., et al. 1995a, Adv. Space Res. 16, 85
Phillips J.L., Bame S.J., Feldman W.C., et al. 1995b, Science 268, 1030
Phillips J.L., Bame S.J., Barnes A., et al. 1995c, Geophysical Research Letters 22, 3301

Phillips J.L., Bame S.J., Feldman W.C., et al. 1996, in : Winterhalter (ed.) Proceedings of the Eighth International Solar Wind Conference (in press)
Roberts D.A. 1989, J. Geophys. Res. 94, 6899
Schwenn R. 1991, in : Schwenn R., Marsch E. (eds.) Physics of the Inner Heliosphere 1 Large- Scale Phenomena. Springer-Verlag, Berlin, p. 99
Smith E.J., Balogh A., Neugebauer M., McComas D. 1995, Geophys. Res. Lett. 22, 3381 Thieme, K.M., Schwenn R., Marsch E. 1989, Adv. Space Res. 9, 127
von Steiger R., Geiss J. 1989, A&A 225, 222
von Steiger R., Wimmer-Schweingruber R.F., Geiss J., Gloeckler G. 1995, Adv. Space Res. 15, 3
Wang Y.-M., Sheeley N.R., Jr. 1990, ApJ 355, 726
Wang Y.-M., Sheeley N.R., Jr. 1995, ApJ 447, L143
Withbroe G.L. 1988, ApJ. 325, 442
Withbroe G.L., Noyes R.W. 1977, ARA&A 15, 363
Yokoyama T., Shibata K. 1995, Nature 375, 42
Zirin H. 1987, Solar Phys. 110, 101
Zirker J. (ed.) 1977, Coronal Holes and High Speed Wind Streams, Col. Assoc. Univ. Press, Boulder, Co.